DOI: 10.1002/ejic.200800303

Sol–Gel Synthesis of Tunable Cerium Titanate Materials

Mónica Martos,*[a] Beatriz Julián-López,[a] José Vicente Folgado,[b] Eloisa Cordoncillo,[a] and Purificación Escribano[a]

Keywords: Sol–gel processes / Cerium / Rare-earth pyrochlore / Titanates / Nanostructures

Cerium titanate structures present a high technological interest because of their optical and catalytic properties. This work reports the synthesis of these materials by a sol–gel methodology that allows mixed oxides with Ti^{IV}/Ce^{III}, Ti^{IV}/Ce^{IV} or Ti^{IV}/Ce^{III}–Ce^{IV} species to be obtained. Crystallization of CeO_2–TiO_2 mixed oxides and $Ce_2Ti_2O_7$ pyrochlore phase was corroborated by XRD and Raman spectroscopy. Magnetic and EPR measurements were performed in order to clarify the oxidation state of the cerium ions in the system as a result of the easy oxidation of Ce^{III}. The firing atmosphere is crucial for the Ce^{III}/Ce^{IV} ratio, which is responsible for the different structure, but it also affects the colouration (yellow, green, brown). This methodology offers the possibility to modulate the Ce^{3+}/Ce^{4+} content and particle sizes providing more ecological coloured pigments based on rare earth elements that could be interesting materials for advanced applications in catalysis.

Introduction

Pyrochlore oxides, $A_2B_2O_7$, are drawing a great deal of attention in many areas of materials science of technological interest because of their, frequently, unique properties induced by a remarkable chemical and structural flexibility.[1–3] Thus, composition electroneutrality can be achieved by a large combination of cation species A and B with different oxidation states, which results in a great variety of physical and chemical properties.[4] Indeed, many properties of pyrochlores are very much influenced by ion distribution and site occupancies.

Among them, rare-earth titanates have become one of the most investigated rare-earth compounds in the past 40 years. Nevertheless, there are only a few investigations on RE-Ti-O systems (RE = rare-earth element) dealing with the preparation of compounds containing RE = cerium. Indeed, it is difficult to prepare Ce^{III} compounds at high temperatures owing to the preference of the Ce^{IV} oxidation state, contrary to the rare-earth elements tendency.

Some cerium titanates exist in the Ce–Ti-O system. Among them is known three cerium titanates involving mainly Ce^{3+},[5] that is, the reddish-brown Ce_2TiO_5 and $Ce_2Ti_2O_7$ and the chestnut $Ce_4Ti_9O_{24}$, and two yellow cerium titanates with mainly Ce^{4+}, $CeTiO_4$ and $CeTi_2O_6$, which are formed when annealing cerium(III) titanates in air at high temperatures.[6] Furthermore, numerous reports have studied the CeO_2–TiO_2 mixed oxide from its catalytic properties.[7–9]

$Ce_2Ti_2O_7$ pyrochlore is formed by Ce^{3+} and Ti^{4+} ions in eight and sixfold coordination, respectively. The ionic radii of Ce^{3+} and Ti^{4+} ions in these coordinate sites are 1.283 and 0.745 Å. These values yield a ratio of 1.72, which is within the tolerated range 1.46–1.8 for the pyrochlore structure.[10] Nevertheless, the oxidation of Ce^{3+} to Ce^{4+} during thermal treatment derived from the intercalation of oxide ions gives species with an ionic radius of 1.11 Å. Because the radii of Ti^{4+} ions in eightfold coordination is 0.88 Å, the radii of the ions on the *A* and *B* sites converge, and the oxide ion distribution more closely approaches that in the fluorite structure. Several characterization techniques were used in order to elucidate the pyrochlore-to-fluorite phase transition after oxidation of a pyrochlore structure.[11,12]

According to the literature,[13] the oxidation of a Ce^{3+} pyrochlore related structure may proceed smoothly at low temperature to maintain the ordered arrangement of the constituent cations, in which both Ce^{3+} and Ce^{4+} cations are randomly distributed. The cerium oxidation process has an important influence in the final properties because of the creation of crystalline defects in the structure. Furthermore, the redox Ce^{3+}/Ce^{4+} couple together with the high capacity to store oxygen of cerium-containing compounds are the basis of the wide application of CeO_2 in heterogeneous catalysis.[14]

The oxidation process may be shown like an intercalation process,[15] which provides the ability to vary the composition and structure of solids in a controlled manner often at

[a] Departmento de Química Inorgánica y Orgánica, Universitat Jaume I de Castellón
Avda. Sos Baynat s/n, 12071 Castellón, Spain
Fax: +34-964-72-82-14
E-mail: mmartos@qio.uji.es
[b] Instituto de Ciencia de los Materiales, Universidad de Valencia Poligono de la Coma s/n, 46980 Paterna-Valencia, Spain

temperatures below those usually used in solid-state synthesis. Furthermore, such metastable intercalation compounds often exhibit unusual but desirable electrical, magnetic and optical properties.

The pyrochlore oxidation has also been researched in the CeO_2–ZrO_2 mixed oxides system. Yashima et al.[16] have reviewed the phase diagram and phase transition in the CeO_2–ZrO_2 system. In the Ce-rich area, a cubic phase is detected; meanwhile, in the Zr-rich area, the monoclinic phase is stabilized. At intermediate compositions, it is proposed the existence of three tetragonal phases with different tetragonal distortion. In addition to the tetragonal phases, a κ-$CeZrO_4$ phase appears by oxidizing the pyrochlore-type $Ce_2Zr_2O_{7+2\delta}$ phase at 873 K;[17] Ce and Zr ions in the κ phase are in an ordered arrangement similar to the arrangement in the pyrochlore-type phase. $CeZrO_4$ fluorite structure is formed by oxygen insertion in the pyrochlore oxygen vacancies and the consequent oxidation of Ce^{3+} to Ce^{4+} ions.

Similar to the appearance of κ-type $CeZrO_4$, $CeTiO_4$ phase results from the insertion of oxygen into the $Ce_2Ti_2O_7$ phase, and the arrangement of the Ce and Ti ions is retained, although the $CeTiO_4$ structure has not been yet clarified. For cerium titanates, the defects related to oxygen, for example, oxygen vacancies, oxygen at interstitial vacancies and holes on the lattice oxygen may be considered as colour centres.[18] This metastable phase could be related to a CeO_2–TiO_2 mixed oxide with 1:1 atomic ratio, which was investigated by Reddy et al. by various techniques.[19,20]

The optical features of cerium makes it a good candidate for colouring applications, as the lowest Ce^{3+} $4f^1 \rightarrow 5d^1$ absorption transition takes place in the blue spectral region that leads to a yellow-orange body colour. As an example, Ce^{3+}-doped garnets present a yellow-orange colour, which indicates that Ce^{3+} was incorporated into the garnets.[21] The blue radiation is strongly absorbed by the allowed $4f \rightarrow 5d$ transition of Ce^{3+}, which leads to a yellow $5d \rightarrow 4f$ (to the spin-orbit split $^2F_{7/2}$ and $^2F_{5/2}$ levels) emission band.[22] The colouration of titanates was ascribed to charge-transfer transitions in which an electron is transferred from the metal ion to the empty $3d$ orbitals of the Ti^{4+} ion. In contrast, the presence of Ce^{IV} ions can generate charge-transfer bands that are also related to the colour mechanism, which, in this case, a yellow colouration.

The conventional solid-state reaction traditionally used for the preparation of these materials involves laborious heating cycles at high temperatures with repeated grinding of the component oxides. The resulting powders show extensive agglomeration and compositional heterogeneity. However, electrical and optical properties are strongly influenced by the particulate morphology and compositional homogeneity. In order to avoid these problems, several chemical synthetic methods for the rare earth pyrochlores have been developed.[23–25] The principal benefits of solution synthesis techniques in contrast to conventional high-temperature solid-state reactions include the high chemical homogeneity achieved on the molecular scale in the solution. Among many methods, sol–gel synthesis is particularly promising for production of materials without the need of high-temperature calcination that influence the final properties of the product.[26,27]

Concerning these structures, the present study is aimed to obtain cerium titanate compounds as alternative colouring materials to substitute the highly toxic lead, cadmium, chromium and nickel pigments commonly used in the ceramic industry. This work stresses the synthetic methodologies (sol–gel route) that allow mixed oxides with Ti^{IV}/Ce^{III}, Ti^{IV}/Ce^{IV} or Ti^{IV}/Ce^{III}–Ce^{IV} species to be obtained. A structural, magnetic and spectroscopic characterization of these materials is performed.

Results and Discussion

Figure 1 depicts the diffractograms of the samples fired in air at different temperatures. It can be observed that at low temperatures (700 and 800 °C) there is a unique phase corresponding to the CeO_2 structure (JCPDS 78-694). However, at 1000 and 1200 °C, TiO_2 rutile (JCPDS 78–1510) appears as a secondary phase, which indicates the crystallization of TiO_2 at high temperatures. This behaviour was already reported by Fang et al.[28] They propose a reaction mechanism on TiO_2–CeO_2 mixed oxides on the basis of the formation of a Ti:CeO_2 solid solution at low temperature, which presents a low crystallinity of the TiO_2 anatase; therefore, the XRD pattern only displays the typical pattern of CeO_2 with a cubic fluorite structure.

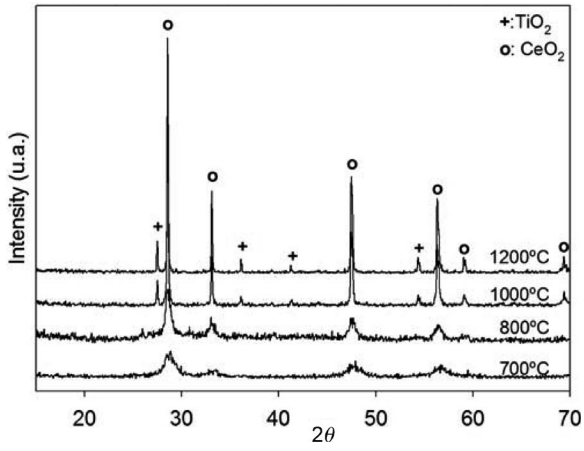

Figure 1. XRD of the samples fired at different temperature.

In our system, titanium ions could be either inside the CeO_2 structure as a solid solution, but no significant shift in the diffraction peaks was detected, or the ions could be an amorphous or nanocrystalline anatase material.

The appearance of the CeO_2 phase detected by XRD implies an oxidation of Ce^{3+} precursor species to Ce^{4+} ions. The broad peaks observed in the powder XRD pattern (likely the result of limited crystallinity because of the relatively low temperatures necessary to access the phase), as well as a non-negligible background (likely originating from some residual amorphous intermediate) make structure refinement difficult.

Table 1 lists the unit-cell parameters of CeO_2 calculated from the XRD data according to a CeO_2 fluorite structure (space group $Fm\bar{3}m$) by using the WinXPow program.[29] The unit-cell parameters of cubic CeO_2 in the mixed oxide are, at all temperatures, a little bit smaller than that of pure CeO_2, which is indicative of some kind of shrinkage of the cubic CeO_2 unit cell. This in turn indicates the incorporation of Ti^{IV} ions. Thus, the interaction between the octahedral Ti in TiO_2 and the eightfold coordination of the Ti in CeO_2 will inhibit crystallization of rutile until high temperature.[30] At 1000 and 1200 °C, the CeO_2 cell volume is more similar to that of pure CeO_2 than that at lower temperature, which indicates that Ti ions in solid solution migrate from CeO_2 to crystallize as TiO_2 rutile phase.

Table 1. Crystalline size and calculated lattice parameter *a* at different firing temperatures.

Temperature [°C]	*a* [Å]	Crystalline size [nm]
700	5.380(3)	7.34
800	5.4011(15)	18.20
1000	5.40723(19)	51.89
1200	5.4065(4)	105.93
CeO_2 fluorite	5.411(5)	17.09

From the (1 1 1) diffraction peak of fluorite CeO_2, the average crystallite sizes of the CeO_2 particles were calculated by using the Debye–Scherrer formula, and they are summarized in Table 1. The values confirm a continuous increase in particle size with temperature that ranges from ≈7 nm (700 °C) to 105 nm (1200 °C).

The morphology and compositional homogeneity of the particles were studied by SEM analysis. Special attention was paid to the samples in which Ti species were not detected by XRD. Figure 2 displays a SEM micrograph, the representative elemental maps of Ti and Ce and an elemental analysis spectrum of the powders fired at 700 °C under air. The SEM image shows that cerium titanate particles are found in the micrometric scale and do not present any specific morphology. Elemental analysis performed by energy dispersive X-ray (EDX) showed a homogeneous distribution of the elements in the analyzed regions, which correspond to the initial stoichiometry. Moreover, the mapping images indicate that, within the magnification used, no Ti and Ce segregated particles are detected, as both elements present a uniform distribution, which supports the formation of a Ce–Ti solid solution.

The evolution of the oxygen sublattice with temperature was analyzed by Raman spectroscopy. Figure 3 shows the Raman spectra recorded for the samples after different heat treatments. All the spectra present an important Raman band around 460 cm^{-1}, which can be attributed to the Raman-active mode of CeO_2 with the F_{2g} symmetry. According to theoretical calculations, the cubic CeO_2 structure possesses six optical-phonon branches, but only one vibration around 463 cm^{-1} (symmetric breathing of the oxygen ions around Ce ions) is generally detected by spectral measurements,[31] which is in agreement with our results.

The stretching modes of TiO_2 anatase appears at 385, 500 and 625 cm^{-1}.[32] These bands are observed in the spectra recorded up to 800 °C, and all of them disappear at high temperature, which could be attributed to the crystallization of the rutile phase.

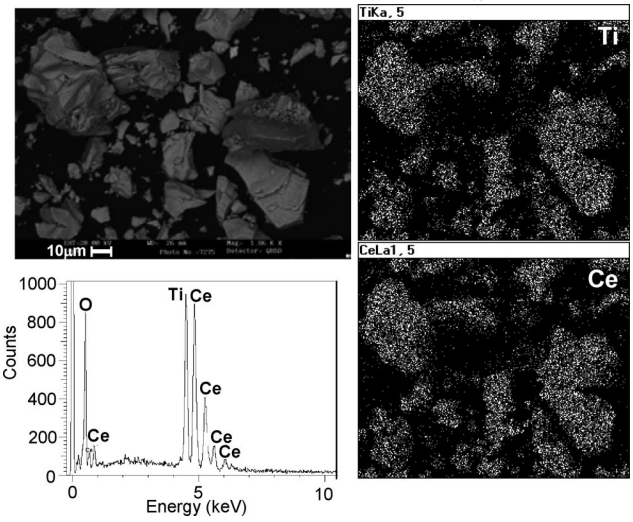

Figure 2. Scanning electron micrograph, Ce and Ti mapping images and EDX spectrum of the sample fired at 700 °C in an air atmosphere.

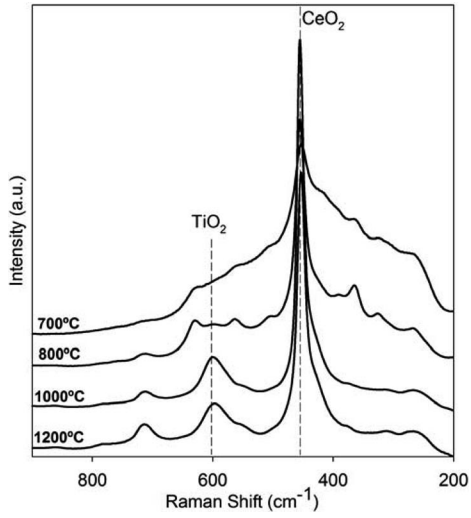

Figure 3. Raman spectra of the samples fired at different temperatures.

In contrast, when the sample is fired at 1000 and 1200 °C, a new band centred around 610 cm^{-1} becomes evident. This vibration could be attributed to the A_{1g} active mode of rutile, for which four Raman modes are allowed [143 (B_{1g}), 447 (E_g), 612 (A_{1g}) and 826 cm^{-1} (B_{2g})].[33,34] Furthermore, a band around 720 cm^{-1} increases in intensity with temperature. This vibrational mode could be assigned to seven-coordinate Ti atoms in a fluorite-like structure,[35] which indicates the incorporation of titanium ions into the fluorite ceria lattice.

Once the structural evolution of the CeO_2–TiO_2 mixed oxide system with temperature was established, the optical properties of the samples were investigated by UV/Vis absorption and luminescence measurements. Figure 4a illus-

trates the variation of the b^* and L^* coordinates, which are the yellow and the intensity components in the CIELAB system, respectively. A linear loss in the yellow component (b^*) of the colour with temperature can be observed, which indicates a regular evolution of the structure; meanwhile, L^* remains almost constant.

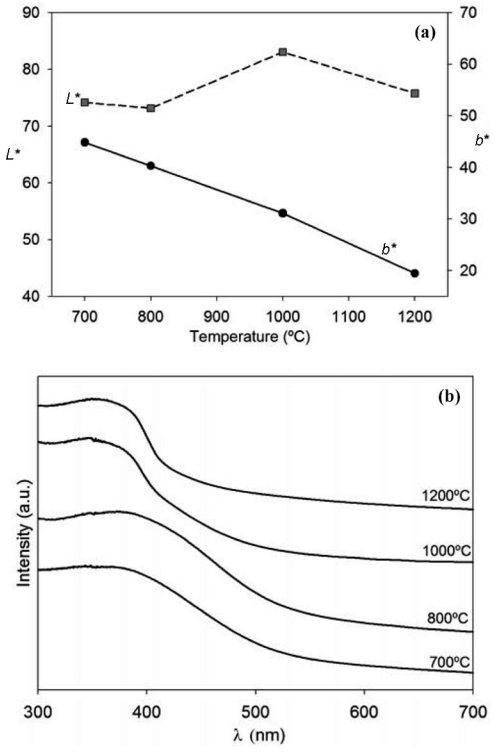

Figure 4. (a) L^* and b^* chromatic coordinates and (b) UV/Vis spectra of the samples with temperature.

The UV/Vis spectra of the samples are depicted in Figure 4b. The spectra exhibit a strong absorption band between 300–400 nm. Despite the fact that rare-earth ions stabilize the trivalent state, as was stated before, cerium compounds usually exhibit the coexistence of Ce^{3+} and Ce^{4+} species because of its particular electronic configuration.[36,37] The electron donation ability of Ce^{III} facilitates the excitation of an electron from the 4*f* to the 5*d* shell, which results in characteristic broad bands in the UV region between 330 and 200 cm^{-1}, although the main absorption band is around 310 cm^{-1}.[38] In contrast, Ce^{IV} favours charge-transfer (CT) transitions from the host ligands to the rare-earth ions. In the case of cerium, 4*f*–5*d* bands of Ce^{3+} ions and the CT bands of Ce^{4+} ions appear in the same wavelength range, which causes them to overlap.[39]

In our samples, the spectra of those fired at low temperatures (700 and 800 °C) show that the band shifts to higher wavenumbers. This difference clearly indicates a modification in the symmetry and chemical environment of the active cerium ions. We have to bear in mind that at low temperatures, the CeO_2 fluorite structure is partially occupied by Ti ions, both located in cubic positions. Because the ionic radius of Ce^{4+} ions is larger than that of Ti^{4+} ions, the unit cell shrinks and Ce ions possess a constricted environment, which makes the Ce–O bond covalence higher than that in a regular cubic structure. The higher covalent character reduces the interaction between the electrons, as they spread out over wider orbitals, and electronic transitions require lower energy, which leads to the shift in absorption bands at longer wavelengths.

In contrast, the absorption spectra seem to possess two bands that could be assigned to the presence of Ce^{3+} and Ce^{4+} ions simultaneously. Therefore, because of the overlap of both bands, it is really difficult to determine what species is responsible for the colour with this optical technique.

Ce^{III} ions ($4f^1$) present a characteristic intense-blue emission upon UV excitation because of a radiative transition from the excited 5*d* level to the ^2F ground state of the ions.[40] Therefore, in order to corroborate the presence of Ce^{3+} ions, the fluorescence of the samples was performed. Figure 5 depicts representative excitation and emission spectra of the sample fired at 700 °C. At all temperatures tested in the present study, the samples presented similar luminescence behaviour, which strengthens the existence of trivalent ions in all cases. The excitation spectrum for λ_{em} = 363 nm shows a band at 266 nm, which corresponds to optical transitions from the $^2F_{5/2}$ ground state to some of the five higher-lying levels of the ^2D excited state of Ce^{3+} in the crystal.[41,42] The emission spectrum recorded upon λ_{exc} = 266 nm shows the characteristic emission band at 363 nm, which corresponds to the parity-allowed electric-dipole transition 5*d*–4*f* after the nonradiative relaxation process inside the nondegenerate ^2D lying levels.[43]

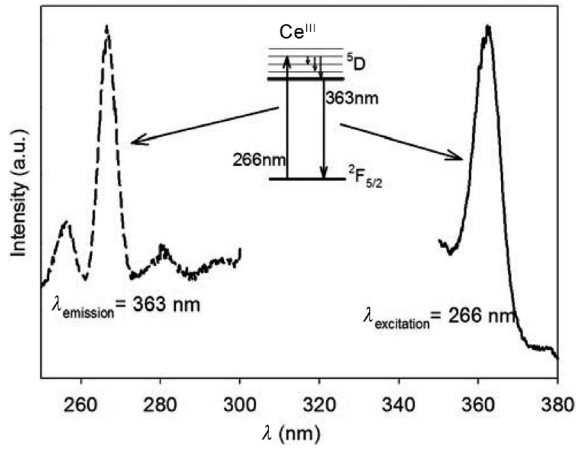

Figure 5. Emission and excitation spectra of the sample fired at 700 °C in air.

Although the existence of Ce^{III} was evidenced from the optical results, there is significant oxidation to Ce^{IV} during thermal treatment in air that leads to the crystallization of CeO_2 and TiO_2. Therefore, in order to obtain the desired $Ce_2Ti_2O_7$ phase, the samples were fired under a reducing atmosphere.

Fired Under Reducing Conditions

In order to prevent the oxidation of Ce^{III} to Ce^{IV} during firing, the sample was fired at 700 and 1000 °C under re-

ductive conditions under a N_2–glucose atmosphere. XRD results showed that a N_2–glucose atmosphere does not prevent oxidation towards CeO_2, as no differences with the samples fired in air were found in the XRD patterns at 700 and 1000 °C for 2 h (not shown). Nevertheless, the samples presented a greenish colouration indicative of some kind of change in the species responsible for the colour, possibly due to the existence of a higher concentration of trivalent species, which highly affect the final colour.

In order to elucidate the final oxygen content and the oxidation state of the metallic ions, EPR and magnetic measurements were carried out. We assume all the studied samples have a composition between pyrochlore $Ce_2Ti_2O_7$ and fluorite $Ce_2Ti_2O_8$. Weak EPR signals are observed only for temperatures lower than 50 K. Figure 5 presents the observed spectra at 10 K. For the raw sample, a very broad axial signal is observed covering practically the entire magnetic field measured (10000 G), although it can be interpreted with $g_{\|}$ approx. 1.0 and $g_{\perp}$ approx. 2.3. A similar but less intense signal is observed in the spectra of samples fired at 700 °C under a N_2–glucose atmosphere, whereas it is nearly absent in the spectra of the samples fired at 700 and 1000 °C in air and at 1000 °C under N_2–glucose. This signal could be attributed to the presence of Ce^{3+} ions in the samples rather than Ti^{3+}; hence, narrow signals at g values close to 2.0 are expected for this ion.[44] In fact, the spectra are very similar to those reported by Misra[45] for Ce^{3+} doped in $Y(NO_3)_3{\cdot}6H_2O$ crystals and by Scotti[46] in Ce-doped phosphosilicate glasses. In both cases it was postulated that Ce^{3+} ions occupy many distorted octacoordinated sites, with a strong mixing of the various Kramer's doublets arising from the $^2F_{5/2}$ ground state. Furthermore, as the intensity of this signal decreases on going from the raw to the samples fired at 1000 °C, it is expected that the concentration of the Ce^{3+} ions in the samples also decreases in the same sense (see below). This result points to the instability of Ce^{3+} species in air with increasing firing temperatures, with the result of its oxidation to Ce^{IV} and the formation of CeO_2. Taking into account that the initial species are Ce^{III} and Ti^{IV}, we could expect the following redox process:[5] $Ce^{3+} + Ti^{4+} \rightarrow Ce^{4+} + Ti^{3+}$. The oxidation of Ce^{III} without the appearance of an appreciable amount of Ti^{III} ions could be explained according to the following crystallization mechanism: Ce^{III} ions tend to segregate and diffuse towards the surface of the Ce–Ti mixed oxide during heat treatment. This effect was already demonstrated by XPS measurements[47] and fractal analysis[9] of a series of CeO_2–TiO_2 samples. Thus, the cerium species mainly located at the surface of the particles are more accessible than the internal titanium species, and they can be involved in redox processes with the furnace atmosphere.

A weak signal centred at a g value of 6.8 is fully resolved in the "1000" samples. It consists of a narrow feature exhibiting weaker hyperfine satellites ($|A| = 227 \times 10^{-4}$ cm^{-1}) from a nucleus having nuclear spin I = 7/2 (Figure 6, bottom). This set of signals are unambiguously assigned to an impurity of Er^{3+} (^{167}Er isotope abundance is 23%, I = 7/2) in cubic sites.[48]

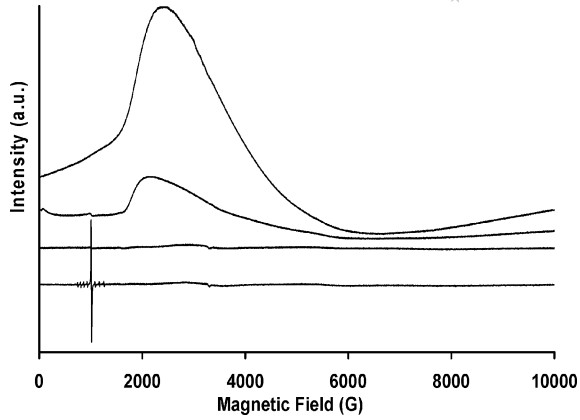

Figure 6. EPR spectra of the studied samples at 10 K. From top: raw, 700N_2–glucose, 700 and 1000 °C.

Magnetic measurements results are summarized in Figure 7 as a plot of the product of the susceptibility per mol of Ce and temperature versus temperature. The raw sample is clearly paramagnetic and follows a Curie–Weiss law.

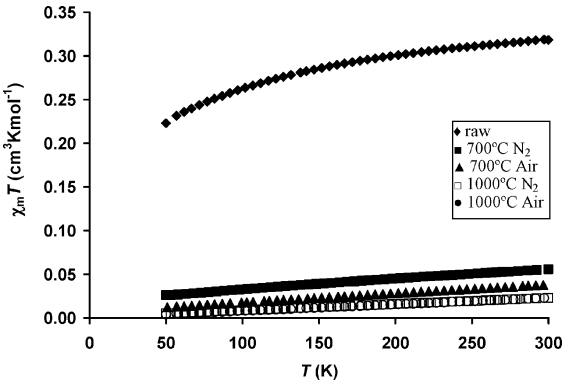

Figure 7. Plot of experimental $\chi_m T$ for the studied samples.

From the EPR data we can assume that paramagnetism is due only to Ce^{3+}; hence, the decrease in the $\chi_m T$ product with decreasing temperature is easily understood by the depopulation of the higher-energy Kramer's doublets arising from the crystal-field splitting of the ground state of the lanthanide ion, $^2F_{5/2}$, as observed in most Ce^{III} compounds.[49] Nevertheless, the observed $\chi_m T$ product at room temperature is lower than that expected for the free ion (0.79 cm^3 mol^{-1} K) or that observed in Ce_2O_3 (0.52 cm^3 mol^{-1} K).[51,52] The last value has been used by several authors[50–53] to evaluate the percentage of paramagnetic Ce^{3+} centres in cerium oxides. Accordingly, taking into account that the sol–gel procedure does not modify the amounts of Ce and Ti introduced as precursors (the stoichiometric formula), we can estimate that the Ce^{3+} content of the raw sol–gel sample is approximately 60%, which leads to a formula of $Ce_2Ti_2O_{7.4}$. The other samples have much less paramagnetism and the majority of the cerium is in the tetravalent state. From the susceptibility data we can extract the results indicated in Table 2, which are in full accord with the intensity of the signals observed in the EPR spectra.

Table 2. Ce^{III} percentage and calculated formula according the susceptibility data.

Sample	Ce^{III} percentage	Formula
Raw	60	$Ce_2Ti_2O_{7.4}$
$700N_2$	12	$Ce_2Ti_2O_{7.88}$
700	7	$Ce_2Ti_2O_{7.93}$
$1000N_2$	4	$Ce_2Ti_2O_{7.96}$
1000	2	$Ce_2Ti_2O_{7.98}$

According to the obtained results it was concluded that the N_2–glucose atmosphere is not reductive enough to avoid the oxidation of Ce^{III}. Thus, a more powerful reducing agent such as H_2 was tested. XRD analysis showed interesting changes in the product phases (Figure 8).

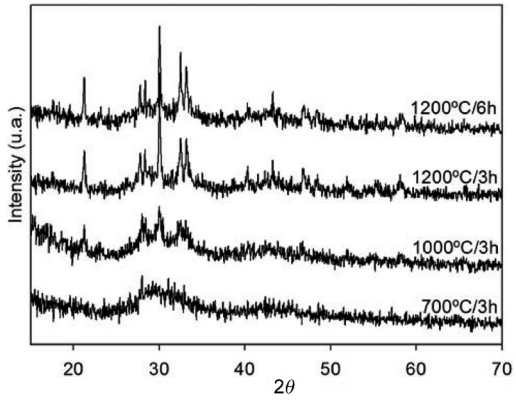

Figure 8. XRD patterns of the samples fired under a N_2–H_2 atmosphere.

At 700 °C, XRD pattern shows the typical feature of an amorphous material. At 1000 °C, an incipient crystallization is observed; however, it is not until 1200 °C that the diffraction peaks can be identified with the $Ce_2Ti_2O_7$ pyrochlore phase (JCPDS 47-667). This structure indicates that the cerium ions are mainly in the trivalent oxidation state. Comparing these patterns with those obtained under an oxidizing atmosphere, a lower crystallinity can be observed. This fact indicates that the amorphous phase (not detected by XRD) still coexists with the well-crystallized pyrochlore structure. A possible reason for this low crystallinity could be attributed to the poor amount of oxygen available in the furnace atmosphere, which acts not only to inhibit Ce^{III} oxidation but also to delay the crystallization process. The difficulty to crystallize $Ce_2Ti_2O_7$ compounds from an amorphous Ti^{IV}–Ce^{III} mixed oxide has already been reported.[47] Rietveld refinements cannot be conducted, because of the low crystallinity of the samples and the poor definition of the XRD patterns.

The study of the bond vibrations by Raman spectroscopy corroborates the differences in the structures developed under different atmospheres. Figure 9 depicts the Raman spectra after firing at 1000 °C in air and reducing atmospheres. It can be seen that the sample fired under H_2 presents a different spectrum than the other two spectra and develops bands corresponding to the CeO_2 and TiO_2 rutile vibration mode at 460 and 610 cm^{-1}, respectively.

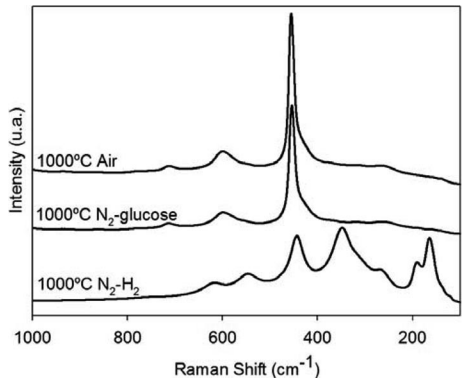

Figure 9. Raman spectra of the samples fired at 1000 °C.

It can be observed that the spectrum recorded for the H_2-treated sample is not dominated by the bands of the Ce–O (in CeO_2) and Ti–O (in TiO_2) vibrations located at 460 and 610 cm^{-1}, respectively. An important change in the profile is detected with appearance of new bands at 165, 190, 350 and 545 cm^{-1}, which can be attributed to the $Ce_2Ti_2O_7$ structure.[54]

Magnetic measurement results for the best-crystallized $Ce_2Ti_2O_7$ sample (calcined at 1200 °C/6 h under H_2) is represented in Figure 10. It is easily observed that the sample treated at 1200 °C is more paramagnetic than those reported in Figure 7. As set out above, we assume that paramagnetism is due mainly to Ce^{3+} and, hence, the decrease in the $\chi_m T$ product with decreasing temperatures arises from depopulation of the higher-energy Kramer's doublets. Assuming the same considerations stated above, we can estimate that the percentage of paramagnetic Ce^{3+} centres in the samples treated at 1000 °C/3 h H_2 (not shown) is about 20%, which leads to a formula of $Ce_2Ti_2O_{7.8}$. Nevertheless, the observed room-temperature $\chi_m T$ product for samples treated at 1200 °C/H_2 for 3 and 6 h is 0.53 and 0.58 $cm^3 mol^{-1} K$, respectively, which is somewhat higher than the previously cited value of 0.52 $cm^3 mol^{-1} K$.[51,52] These results could be understood by considering that all

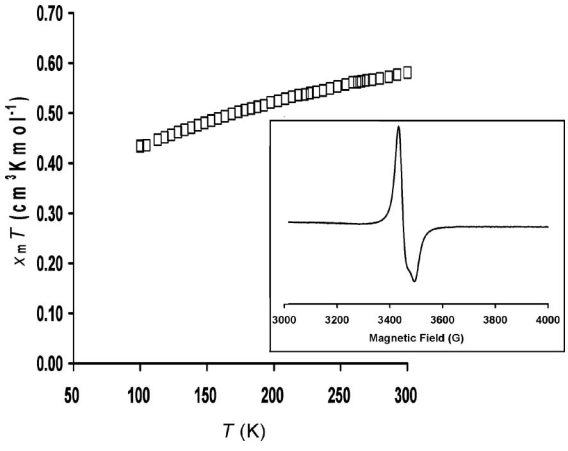

Figure 10. Plot of experimental $\chi_m T$ for the H_2 treated sample fired at 1200 °C/6 h. Inset: central part of the EPR spectra of the same sample registered at 5 K.

the cerium is in the trivalent state and that there is some additional contribution due to the presence of small amounts of titanium also in the trivalent state. In an approximate analysis, by considering the d^1 configuration of Ti^{3+} and the expected spin-only contribution to paramagnetism, we could estimate a percentage of 2 and 16% of trivalent titanium in those samples, which leads to compositions of $Ce_2Ti_2O_{6.98}$ and $Ce_2Ti_2O_{6.84}$, respectively.

These considerations are fully confirmed by EPR measurements (see inset of Figure 10). In fact, the low-temperature spectrum of a sample treated at 1200 °C/6 h under an H_2 atmosphere exhibits new features that are not observed in the spectra of the samples studied above or in the sample treated at 1000 °C under H_2. It consists of weak axial signals with $g_\perp = 1.97$ and $g_\parallel = 1.94$. This kind of spectrum and those g values were assigned in the literature to the presence of Ti^{3+} defects in the rutile TiO_2 phases,[55–57] which confirms the presence of trivalent titanium in our samples.

The use of reductive atmospheres also produces important changes in the body colour of the samples. Table 3 details the different chromatic coordinates of the samples fired under oxidative and reductive atmospheres at 700, 1000 and 1200 °C. When the sample is fired in air, it presents a yellow colouration that originates from the O2*p*–Ce4*f* charge-transfer transitions, which changes to a green or brown shade after firing under N_2–glucose or N_2–H_2, respectively. In the case of the calcination with N_2–glucose, the colouration at 1000 °C is quite similar to the one treated in air, which agrees with the higher rate of Ce^{III} oxidation and the crystallization of TiO_2 as shown by XRD. According to these results, the changes in colouration could be related to the different oxidation state of the cerium ions in the samples or to oxygen defects that act as colour centres.

Table 3. Chromatic coordinates of samples fired under different heat treatments.

Temperature [°C]	Atmosphere	*L**	*a**	*b**
700	Air	74.2	4.9	44.9
700	N_2–glucose	47.6	–0.1	11.1
700	N_2–H_2	51.4	–1.7	10.9
1000	Air	83.1	–1.3	31.1
1000	N_2–glucose	80.3	–0.5	20.7
1000	N_2–H_2	53.5	1.5	14.4
1200	Air	75.8	2.1	19.4
1200	N_2–H_2	46.6	5.6	11.4

As conclusion, the $Ce_2Ti_2O_7$ structure was obtained by sol–gel methodology at a lower temperature (1000 °C/3 h) than those reported by others[1,18,58] (1200–1300 °C for several days). It was demonstrated that the firing process is crucial for the development of the pyrochlore phase, as Ce^{III} is easily oxidized to Ce^{IV}. Thus, calcination at 1000 °C in air or with the use of soft reducing agents (CO from glucose–N_2 flow) are conducive to CeO_2 and TiO_2 crystallization; meanwhile, with a H_2(5%)-N_2 flow, the pyrochlore structure is obtained.

The possibility to modulate the Ce^{3+}/Ce^{4+} content depending on the firing atmosphere is an important feature for applications in the catalysis and optical fields. The catalytic response will be further investigated. This behaviour, together with the small particle sizes of the powders, makes these compounds potential materials in multifunctional applications.

Conclusions

This paper reports the synthesis of a rare-earth-containing pyrochlore system $Ce_2Ti_2O_7$. Crystallization of the pyrochlore phase was corroborated by XRD and Raman spectroscopy. Magnetic and EPR measurements were performed in order to clarify the oxidation state of the cerium ions in the system. The $Ce_2Ti_2O_7$ structure was obtained by sol–gel methodology under relatively soft conditions while under a reducing atmosphere. It was demonstrated that the firing treatment is crucial for the development of the pyrochlore, as Ce^{III} is easily oxidized to Ce^{IV}. Thus, calcination in air or with the use of soft reducing agents leads to CeO_2–TiO_2 compositions (including solid solutions) with yellow-to-green colourations. In contrast, with the use of an aggressive reducing agent such as H_2, the pyrochlore structure is obtained, and the colour changes to brownish shades. The oxidation of trivalent to tetravalent cerium ions is compensated by oxygen vacancies, which can cause distortion of the crystal lattice affecting the physical, chemical and optical properties of the final product. The possibility to modulate the Ce^{3+}/Ce^{4+} content and particle sizes depending on the firing conditions (temperature and atmosphere) is interesting for applications in the catalysis and optical fields. The methodology reported in this work allows the development of a more ecological coloured material based on rare-earth elements and a promising catalytic material.

Experimental Section

General: The cerium titanate structure was prepared by sol–gel methodology by using $Ce(NO_3)_3{\cdot}6H_2O$ and titanium isopropoxide as precursors in a stoichiometric amount and absolute ethanol as the solvent. The great reactivity of titanium isopropoxide requires that the synthesis be processed with strict control of moisture and conditions of hydrolysis in order to prepare homogeneous gels rather than precipitates. In this sense, in order to control the hydrolysis and condensation reactions of titanium and cerium species, the chemical modification with a chelating ligand such as acetyl acetone (acac) was performed in a preliminary study. The role of acac in the solution is to prevent the hydrolysis of Ti^{IV} through less hydrolyzable M–acac bonds.[59,60] Different Ti/acac ratios were tested for obtaining transparent gels, and it was concluded that the optimal conditions involved a 4:1 ratio of Ti/acac. Thus, once dissolved the cerium precursor in ethanol, acac and titanium isopropoxide were added dropwise with continuous stirring to the latter solution. The respective concentrations of Ce and Ti were both 0.15 M.[61]

After that, the mixture was heated at reflux (70 °C) for 24 h under a nitrogen atmosphere in order to preserve the solution from the

atmosphere humidity. The resulting orange sol led to a transparent gel after evaporation of solvent, which became a powder after drying under IR lamps. The obtained powders were fired under fluxes of different atmospheres (air, N_2–glucose and H_2–N_2) at 700, 800, 1000 and 1200 °C with an annealing time of 2 h in a Nabertherm electric furnace at a heating rate of 5 °C min^{-1}. The calcination with reductive conditions were carried out in a tubular furnace with a gas flow [N_2 or H_2(5%)–N_2]. In the calcination under N_2–glucose, a crucible filled with glucose was placed in the entrance of the furnace. The oxidized CO/CO_2 products generated from the combustion of the glucose were dragged along the sample with the N_2 flow, which induced the reduction of the sample.

Characterization Techniques: Phase analysis of the fired samples was performed by X-ray powder diffraction (XRD) with a SIEMENS D5000 diffractometer with Cu-K_α radiation. Data were collected by step-scanning from 15 to 70° 2θ with a step size of 0.05° 2θ and 1.5 s counting time at each step. The goniometer was controlled by the "SIEMENS DIFFRACT plus" software, which also determined diffraction peak positions and intensities. The instrument was calibrated by using an external Si standard. Raman spectra were recorded with spectral windows of 3500–100 cm^{-1} with a Raman Perkin–Elmer System 2000 spectrometer. UV/Vis/NIR spectroscopy and a colorimetric study of the samples were carried out with a CARY 500 SCAN VARIAN spectrophotometer in the 300–1100-nm range. The diffuse reflectance spectra (DRS) were obtained by using an integrating sphere and $BaSO_4$ as reference. The CIELAB colour parameters $L^*a^*b^*$ were determined by coupling an analytical software for colour measurements to the VARIAN spectrophotometer. The data were registered from 380 to 700 nm by using a PTFE blank as reflecting standard and a D65 standard illuminant. The chromatic coordinates of the samples were compared with those of a commercial pink pigment used in the ceramic industry. In the CIELAB system, L^* is the lightness axis [black (0) to white (100)], a^* is the green (<0) to red (>0) and b^* is the blue (<0) to yellow (>0) axis.[62,63] Scanning electron micrographs of the samples were taken with a scanning electron microscope (SEM) Leica, Leo 440 model, equipped with a spectrometer of Energy Dispersion of X-ray (EDX) from Oxford instruments by using the following operational parameters: acceleration voltage 20 kV, measuring time 100 s, working distance 25 mm, counting rate 1.2 kcps. The samples for microstructural and microanalysis determinations were deposited in an aluminium holder and coated by graphite film. Polycrystalline powder EPR (X-band, 9.47 GHz) spectra were recorded with a Bruker E580 spectrometer from room temperature to 5 K. Variable-temperature susceptibility measurements were carried out in the temperature range 50–300 K at an applied magnetic field of 0.1 T on polycrystalline samples with a Quantum Design MPMS-XL-5 SQUID magnetometer. The susceptibility data were corrected for the sample holder previously measured by using the same conditions and for the diamagnetic contributions as deduced by using Pascal's constant tables.

Acknowledgments

This research was supported by the Spanish Government (MEC: MAT-2005–00541) and Bancaixa Foundation-Universitat Jaume I (P1 1B2007-47) projects. M. M. and B. J.-L. specially thank the UJI and MEC for their PhD fellowship and "Ramon y Cajal" program, respectively.

[1] A. V. Shyakhtina, A. V. Levchenko, J. C. C. Abrantes, V. Yu. Bychkov, V. N. Korchak, V. A. Rassulov, L. L. Larina, O. K. Karyagina, L. G. Shcherbakova, *Mater. Res. Bull.* **2007**, *42*, 742.
[2] A. R. West, *Solid State Chemistry and Its Applications*, Wiley, Chichester, **1985**.
[3] J. C. Boivin, G. Mairesse, *Chem. Mater.* **1998**, *10*, 2870.
[4] R. S. Palov, J. B. Carda, V. Blasco, J. M. Hohembergerger, *J. Am. Ceram. Soc.* **2002**, *85*, 1197.
[5] A. Preuss, R. Gruehn, *J. Solid State Chem.* **1994**, *110*, 363.
[6] G. V. Bazuev, O. V. Makarova, V. A. Zhilyaev, G. P. Shveikin, *Russ. J. Inorg. Chem.* **1976**, *21*, 1447.
[7] B. M. Reddy, A. Khan, P. Lakshmanan, M. Aouine, S. Loridant, J. C. Volta, *J. Phys. Chem. B* **2005**, *109*, 3355.
[8] M. F. Luo, J. Chen, L. S. Chen, J. Q. Lu, Z. C. Feng, C. Li, *Chem. Mater.* **2001**, *13*, 197.
[9] T. López, F. Rojas, R. Alexander-Katz, F. Galindo, A. Balankin, A. Buljan, *J. Solid State Chem. B* **2004**, *177*, 1873.
[10] J. B. Thomson, A. R. Armstrong, P. G. Bruce, *J. Am. Chem. Soc.* **1996**, *118*, 11129.
[11] M. Glerup, O. F. Nielsen, F. W. Polsen, *J. Solid State Chem.* **2001**, *160*, 25.
[12] T. Omata, M. Kita, S. Otsuka-Yao-Matsuo, M. Katada, *J. Phys. Chem. Solids* **2005**, *66*, 53.
[13] H. Kishimoto, T. Omata, S. Otsuka-Yao-Matsuo, K. Ueda, H. Hosono, H. Kawazoe, *J. Alloys Compd.* **2000**, *312*, 94.
[14] W. C. Marckrodt, M. Fowles, M. A. Morris, *European Patent 91.307.165*, **1991**.
[15] R. Higashinaka, H. Fukazawa, Y. Maeno, *Phys. Rev. B* **2003**, *68*, 014415.
[16] M. Yashima, M. Takashina, M. Kakihana, M. Yoshimura, *J. Am. Ceram. Soc.* **1994**, *77*, 1869.
[17] S. Otsuka-Yao, H. Morikawa, N. Izu, K. Okuda, *J. Jpn. Inst. Met.* **1995**, *59*, 1237.
[18] S. Otsua-Yao-Matsuo, T. Omata, M. Yoshimura, *J. Alloys Compd.* **2004**, *376*, 262.
[19] B. M. Reddy, A. Khan, Y. Yamada, T. Kobayashi, S. Lorindant, J. C. Volta, *J. Phys. Chem. B* **2003**, *107*, 5162.
[20] B. M. Reddy, P. Lakshmanan, A. Khan, *J. Phys. Chem. B* **2004**, *108*, 16855.
[21] A. A. Setlur, W. J. Heward, Y. Gao, A. M. Srivastava, R. G. Chandran, M. V. Shankar, *Chem. Mater.* **2006**, *18*, 3314.
[22] G. Blasse, A. Bril, *Appl. Phys. Lett.* **1967**, *11*, 53.
[23] X. Gong, P. Wu, W. Chen, H. Yang, *J. Mater. Res.* **1998**, *13*, 469.
[24] D. Chen, R. Xu, *Mater. Res. Bull.* **1998**, *33*, 409.
[25] M. A. Subramanian, *Mater. Res. Bull.* **1992**, *27*, 939.
[26] M. Martos, B. Julián, H. Dehouli, D. Gourier, E. Cordoncillo, P. Escribano, *J. Solid State Chem.* **2007**, *180*, 679.
[27] M. Martos, B. Julián-López, E. Cordoncillo, P. Escribano, *J. Phys. Chem. B* **2008**, *112*, 2319.
[28] J. Fang, X. Bi, D. Si, Z. Jiang, W. Huang, *Appl. Surf. Sci.* **2007**, *253*, 8952.
[29] Stoe & Cie, *STOE WinXPOW (Version 1.06)*, Stoe & Cie GmbH, Darmstadt, Germany, **1999**.
[30] K. J. Hadjiivanov, D. G. Kissurski, *Chem. Soc. Rev.* **1996**, *25*, 61.
[31] W. H. Weber, K. C. Hass, J. R. McBride, *Phys. Rev. B* **1993**, *48*, 178.
[32] S. T. Martin, C. L. Morrinson, M. R. Hoffmann, *J. Phys. Chem.* **1994**, *98*, 13695.
[33] A. Orendorz, A. Brodyanski, J. Lösch, L. H. Bai, Z. H. Chen, Y. K. Le, C. Ziegler, H. Gnaser, *Surf. Sci.* **2007**, *601*, 4390.
[34] S. P. S. Porto, P. A. Fleury, T. C. Damen, *Phys. Rev.* **1967**, *154*, 522.
[35] K. J. Moreno, A. F. Fuentes, M. Maczka, J. Lanuza, U. Amador, *J. Solid State Chem.* **2006**, *179*, 3805.
[36] A. Pepe, M. Aparicio, S. Ceré, A. Durán, *J. Non-Cryst. Solids* **2004**, *348*, 162.
[37] K. Annapurna, R. N. Dwivedi, P. Kundu, S. Buddhudu, *Mater. Lett.* **2004**, *58*, 787.
[38] G. U. Zhenan, *J. Non-Cryst. Solids* **1982**, *52*, 337.

[39] H. Ebendorff-Heidepriem, D. Ehrt, *Opt. Mater.* **2000**, *15*, 7.
[40] L. Huang, X. Wang, H. Lin, X. Liu, *J. Alloys Compd.* **2001**, *316*, 256.
[41] G. Blasse, B. Grabmaier, *Luminescent Materials*, Springer, Berlin, **1994**.
[42] C. Q. Xu, Z. X. Zheng, W. H. Tang, Y. C. Wu, *J. Lumin.* **2007**, *124*, 151.
[43] E. Cordoncillo, F. J. Guaita, P. Escribano, C. Philippe, B. Viana, C. Sanchez, *Opt. Mater.* **2001**, *18*, 309.
[44] B. A. Goodman, J. B. Raynor, *Adv. Inorg. Chem. Radiat.* **1970**, *13*, 136.
[45] S. K. Misra, S. Ibor, *Physica B* **1998**, *253*, 111.
[46] C. Canevali, M. Mattoni, F. Morazzoni, R. Scotti, M. Casu, A. Musinu, R. Krsmanovic, S. Polizzi, A. Speghini, M. Betlinelli, *J. Am. Chem. Soc.* **2005**, *127*, 14681.
[47] J. Rynkowski, J. Farbotko, R. Touroude, L. Hilaire, *Appl. Catal A: General* **2000**, *203*, 335–348.
[48] S. A. Al'tshuler, B. M. Kozyrev, *Electron Paramagnetic Resonance in Compounds of Transition Elements*, 2nd ed., John Wiley & Sons, **1974**.
[49] M. Puchalska, J. Mrozinski, J. Legendziewicz, *J. Alloys Compd.* **2008**, *451*, 270.
[50] A. Bensalem, F. Bozon-Verduraz, V. Perrichon, *J. Chem. Soc. Faraday Trans.* **1995**, *91*, 2185.
[51] H. Vidal, S. Bernal, J. Kaspar, M. Pijolat, V. Perrinchon, G. Blanco, J. M. Pintado, R. T. Baker, G. Colon, F. Fally, *Catal. Today* **1999**, *54*, 93.
[52] A. Laachir, V. Perrichon, A. Badri, J. Lamotte, E. Catherine, J. C. Lavalley, J. El Fallah, L. Hilaire, F. Le Normand, E. Quemere, N. S. Sauvion, O. Touret, *J. Chem. Soc. Faraday Trans.* **1991**, *87*, 1601.
[53] J. P. Candy, V. Perrichon, *J. Catal.* **1984**, *89*, 93.
[54] M. T. Vandenborre, E. Husson, J. P. Chatry, D. Michel, *J. Raman Spectrosc.* **1983**, *14*, 63.
[55] C. P. Kumar, N. O. Gopal, T. C. Wang, M. Wong, S. C. Ke, *J. Phys. Chem. B* **2006**, *110*, 5223.
[56] K. Y. Jung, S. B. Park, S. Ihm, *Appl. Catal B* **2004**, *51*, 239.
[57] D. C. Hurum, A. G. Agrios, K. A. Gray, T. Rajh, M. C. Thurnauer, *J. Phys. Chem. B* **2003**, *107*, 4545.
[58] L. A. J. Garvie, H. Xu, Y. Wang, R. L. Putnam, *J. Phys. Chem. Solids* **2005**, *66*, 902.
[59] J. Livage, M. Henry, C. Sanchez, *Prog. Solid State Chem.* **1988**, *18*, 259.
[60] C. J. Brinker, G. W. Scherer, *Sol–Gel Science*, Academic Press, **1990**.
[61] M. Langlet, C. Coutier, J. Fick, M. Audier, W. Meffre, B. Jacquier, R. Rimer, *Opt. Mater.* **2001**, *16*, 463.
[62] P. Escribano, J. B. Carda, E. Cordoncillo, *Esmaltes y Pigmentos Cerámicos, Enciclopedia Cerámica* (3er Tomo), Faenza Editrice Ibérica, Spain, **2001**.
[63] E. J. Dilabert, *Medida del color*; Servicio de Publicaciones, Madrid, Spain, **1982**.

Received: March 25, 2008
Published Online: June 4, 2008

